# Multiple Fault Diagnosis Method in Multistation Assembly Processes Using Orthogonal Diagonalization Analysis

**Zhenyu Kong**
School of Industrial Engineering and Management,
Oklahoma State University,
Stillwater, OK 74078

**Dariusz Ceglarek**
Warwick Manufacturing Group,
University of Warwick,
Coventry, CV4 7AL UK
and Department of Industrial and Systems Engineering,
University of Wisconsin,
Madison, WI 53706

**Wenzhen Huang**
Department of Mechanical Engineering,
University of Massachusetts,
Dartmouth, MA 02747

*Dimensional control has a significant impact on overall product quality and performance of large and complex multistation assembly systems. To date, the identification of process-related faults that cause large variations of key product characteristics (KPCs) remains one of the most critical research topics in dimensional control. This paper proposes a new approach for multiple fault diagnosis in a multistation assembly process by integrating multivariate statistical analysis with engineering models. The proposed method is based on the following steps: (i) modeling of fault patterns obtained using state space representation of process and product information that explicitly represents the relationship between process-related error sources denoted by key control characteristics (KCCs) and KPCs, and (ii) orthogonal diagonalization of measurement data using principal component analysis (PCA) to project measurement data onto the axes of an affine space formed by the predetermined fault patterns. Orthogonal diagonalization allows estimating the statistical significance of the root cause of the identified fault. A case study of fault diagnosis for a multistation assembly process illustrates and validates the proposed methodology.* [DOI: 10.1115/1.2783228]

## 1 Introduction

**1.1 Motivation.** Numerous factors affect product quality in large and complex multistation assembly systems, including dimensional variation control, which can have a significant impact on overall product quality and performance as well as on productivity and production cost. For example, in automotive assembly, fixture-related dimensional faults contribute between 40% and 100% of dimensional failures during the typical four production phases of a new product development, namely, preproduction, launch, one-shift production, and two-shift production [1].

A significant number of fixture failures are related to fixture installation and maintenance. For example, problems related to fixture installation and calibration in the aforementioned four production phases contribute to 5%, 40%, 100%, and 54% of all dimensional faults, respectively [1]. These data indicate that accurate fixture installation and maintenance are crucial for overall product quality, and thus, a great deal of research has focused on: (i) reducing ramp up and/or launch of new products by addressing issues related to fixture fault root cause diagnosis [2–8]; (ii) reducing product changeover by targeting areas related to rapid fixture deployment [9,10]; and (iii) increasing diagnosability through optimal sensor placement [11–14].

In order to monitor and control manufacturing processes, measurement devices such as coordinate measuring machines (CMMs), optical coordinate measuring machines (OCMMs), optical scanners, and datamyte are used extensively for the purposes of data acquisition. With the advancements in sensing and computational technologies, an enormous amount of process- and product-related information is available in real time. Nevertheless, the complexity of assembly systems makes it fairly challenging to diagnose multiple faults in multistation assembly processes, as indicated by [1]. For complex manufacturing systems, such as in the case of automotive and aerospace assembly, solely relying on measurement data for the purpose of localizing root cause of dimensional variation is insufficient. In these cases, it becomes necessary to integrate information related to measurement data as well as product and process models (CAD/CAM).

This need for integration serves as a motivation to develop a model-based rapid root cause identification methodology using interdisciplinary data mining approaches incorporated with CAD/CAM model that can clearly represent the relationship between variations of KCCs and KPCs.

**1.2 Related Research.** In dimensional engineering, fault diagnosis is critical toward identifying root causes that lead to large variation of key product characteristics (KPCs). Because fixture related dimensional faults such as locator position errors and/or wear outs are some of the most significant factors during production phase, they are considered to be the primary error sources in this paper. The summary of related research is presented in Table 1.

All work listed in Table 1 assumes that the deviation of measurement $\mathbf{y}$ has a linear relationship with the deviation of the tolerance contributor $\mathbf{u}$ (for example, fixture locators and/or part mating feature), namely,

$$\mathbf{y} = \mathbf{\Gamma} \cdot \mathbf{u} + \boldsymbol{\varepsilon} \tag{1}$$

where matrix $\mathbf{\Gamma}$ remains constant, and $\boldsymbol{\varepsilon}$ represents the noise in the process. This assumption is valid for dimensional variation analysis because the deviations from design nominal are very small, and thus, in many cases the higher-order components can be dropped based on the Taylor expansion [5].

*1.2.1 Single Station and Single Fault.* Ceglarek and Shi [4] developed a methodology for diagnosis of a single fault in a single-station assembly process by applying principal component analysis (PCA). The geometric relationship, i.e., matrix $\mathbf{\Gamma}$ in Eq. (1), was derived between deviations from design nominal of fixture locators and the measurement points on a panel or a subassembly. This method was enhanced by taking into consideration

Contributed by the Manufacturing Engineering Division of ASME for publication in the JOURNAL OF MANUFACTURING SCIENCE AND ENGINEERING. Manuscript received October 4, 2006; final manuscript received July 23, 2007; published online February 15, 2008. Review conducted by Shivakumar Raman. Paper presented at the 2005 ASME International Mechanical Engineering Congress (IMECE2005), November 5–11, 2005, Orlando, FL.

**Table 1 Related research in fault diagnosis**

| Assembly Systems Type of faults | Single Station | Multistations |
|---|---|---|
| Single fault | Ceglarek and Shi [4,15]<br>Rong et al. [6,16] | Ding et al. [26] |
| Multiple faults | Barton and Gonzalez-Barreto [17]<br>Chang and Gossard [18]<br>Apley and Shi [5,19]<br>Apley and Lee [20]<br>Carlson and Soderberg [21]<br>Camelio and Hu [8] | **Machining:**<br>Zhou et al. [23]<br>Djurdjanovic and Ni [24]<br>**Assembly:**<br>Addressed in this paper |

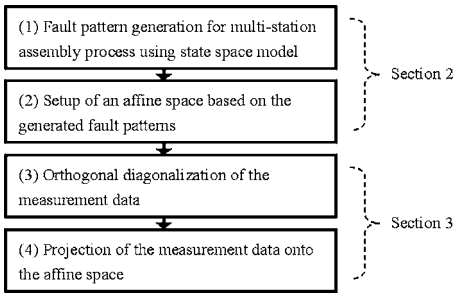


**Fig. 1 Procedure of the proposed method**

the impact of measurement noise on the diagnostic results [15].

Similarly, Rong et al. [6] proposed a diagnostic methodology for dimensional fault diagnosis of compliant beam structures. They obtained matrix $\mathbf{\Gamma}$ by using stiffness matrix of beam structures and applied a least-squares approach to estimate faults within compliant assembly processes. In order to address the issue of ill-conditioning matrix $\mathbf{\Gamma}$, Rong et al. [16] presented an adjusted least-squares approach that is able to overcome the ill-conditioning and produce precise results for certain linear combinations of faults.

*1.2.2 Single Station and Multiple Faults*. Considerable research has been conducted on diagnostic methods for multiple faults in a single-station assembly process. Barton and Gonzalez-Barreto [17] developed process-oriented basis representations for diagnosis of multivariate processes. Process-oriented basis plays the same role as matrix $\mathbf{\Gamma}$. The least-squares method was used to estimate variations of the error sources.

Apley and Shi [5] constructed a fixture fault model using geometric information of the panel and fixture locators and applied a least-squares estimation to identify root causes based on measurement data. This approach relies on a single-station fault model that assumes the complete set of all potential faults can be analytically modeled off line to obtain matrix $\mathbf{\Gamma}$.

Chang and Gossard [18] proposed a computational method for variation fault diagnosis in assembly processes. In their approach, matrix $\mathbf{\Gamma}$ is achieved through simulation of the assembly process and then a least-squares method is applied to estimate variation of root causes.

Data-driven methods, which solely rely on measurement data, have also been applied for diagnostics of manufacturing processes. Apley and Shi [19] proposed a methodology using factor analysis to estimate matrix $\mathbf{\Gamma}$ from measurement data directly without prior knowledge of the faults. Their methodology assumes that matrix $\mathbf{\Gamma}$ has a ragged lower triangular form. Apley and Lee [20] applied independent component analysis to model the fault variation pattern, which assumes that no more than one error source follows a normal distribution. Although advanced statistical and data mining approaches are able to identify some of the important fault patterns in the data, pure data-driven methods suffer from data pattern interpretation in terms of real physical processes, which is critical for root cause diagnosis.

Carlson and Soderberg [21] combined statistical multivariate data analysis with a multifixture single station fault model. They used maximum likelihood estimation to determine the covariance matrix of error sources (fixture locators).

Camelio and Hu [8] presented a designated component analysis (DCA) for dimensional fault diagnosis by predefining a set of fault patterns called designated components using product/process information. In fact, DCA is a special case of the least-squares method, but the generated orthogonal bases using Schmidt transformation are applied for variation estimation, instead of the original designated components.

*1.2.3 Multiple Stations and Single Fault*. Ding et al. [7] applied a state space model to systematically characterize the propagation of fixture fault variation along a multistation assembly process. This method generates a set of predetermined fault patterns for error sources. The developed diagnostic method is an extension of the PCA-based method [4] for single fault diagnosis in a multistation assembly process. The method assumes 2D scenario with all parts being located using "0-2-1" fixturing layouts, i.e., it does not consider part mating feature errors.

*1.2.4 Multiple Station and Multiple Faults*. Aiming at machining processes, Zhou et al. [23] applied a state space approach to formulate a mixed linear model that takes into consideration both mean shift and variation of the processes. For variation estimation, the minimum norm quadratic unbiased estimation (MINQUE) is utilized, which is actually based on maximum likelihood estimation. Djurdjanovic and Ni [24] obtained a linear model using state space representation and the applied Bayesian approach to estimate the covariance matrix of root causes. Their method is a special case of the least-squares approach.

Ding et al. [25] provided a detailed comparison of variation estimation methods used by various fault diagnosis approaches. Essentially, these methods can be classified as either least-squares estimation or maximum-likelihood-based approaches. However, although a significant amount of research has been conducted on diagnostic methodologies, yet to date, there is no systematic methodology available to *diagnose multiple faults in multistation assembly processes*. This paper addresses the current gap in the literature by presenting a new methodology that integrates a state space model with PCA-based orthogonal diagonalization.

**1.3 Proposed Method and Organization of Paper.** Figure 1 illustrates the proposed methodology. First, a generic variation propagation model is developed to generate fault patterns in multistation assembly processes using a state space model. Then an affine space is set up based on the generated fault pattern vectors. The PCA approach is applied to conduct orthogonal diagonalization analysis (ODA) using covariance matrix of the measurement data. By taking advantage of the properties of the ODA, the processed covariance matrix can be projected to each axis of the affine space. The projected length on each axis represents, exactly, the variation of the fault whose pattern is represented by the axis (fault pattern vector). Consequently, the variation of each error source can be estimated.

The rest of the paper is organized in the following format: Section 2 presents a variation propagation model for multistation assembly processes using a state space model. Section 3 proposes a multiple fault identification method using orthogonal diagonalization based on PCA analysis. Section 4 compares the proposed method to the existing approaches. A case study is provided in Sec. 5 to validate the method. Finally, Sec. 6 summarizes the whole methodology.

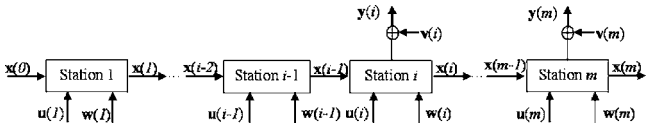


**Fig. 2 Diagram of a multistation assembly process**

## 2 Variation Propagation Model for Multistation Assembly Processes

**2.1 State Space Model for Multistation Variation Propagation.** Figure 2 shows a multistation assembly process with $m$ stations, where variable $i$ represents the station index. State vector $\mathbf{x}(i)$ represents product quality information (e.g., part dimensional deviations) at each station, and inputs $\mathbf{u}(i)$ denote deviations of KCCs, which represent process faults (e.g., fixturing error and part fabrication error). The measurements of KPCs representing product quality are denoted by $\mathbf{y}(i)$, where index $i$ describe the placement of the measurement station (for example, for $i=m$, we have an end-of-line measurement station). Variables $\mathbf{w}(i)$ and $\mathbf{v}(i)$ denote process noise and measurement noise, respectively, and are assumed to be mutually independent.

Part quality at a given current station $\mathbf{x}(i)$ is determined by process error (deviation of KCCs) $\mathbf{u}(i)$, the incoming part quality $\mathbf{x}(i-1)$, and process noise $\mathbf{w}(i)$. Variation propagation can be integrated as a station-indexed state space model [7]

$$\mathbf{x}(i) = \mathbf{A}(i-1)\mathbf{x}(i-1) + \mathbf{B}(i)\mathbf{u}(i) + \mathbf{w}(i) \quad i \in (1,2,\ldots,m) \tag{2}$$

$$\mathbf{y}(i) = \mathbf{C}(i)\mathbf{x}(i) + \mathbf{v}(i) \quad i \in (1,2,\ldots,m) \tag{3}$$

where $\mathbf{A}(i-1)$ is the state matrix, $\mathbf{A}(i-1)\mathbf{x}(i-1)$ represents the effects of product quality from station $(i-1)$ to station $i$, $\mathbf{B}(i)$ is the input matrix, and $\mathbf{B}(i)\mathbf{u}(i)$ represents how product quality is affected by KCCs' deviations at station $i$, and $\mathbf{C}(i)$ is the observation matrix determined by the distribution and number of measurement devices. Based on Eqs. (2) and (3), the relationship between process error sources $\mathbf{u}(i)$ and end-of-line measurement $\mathbf{y}(m)$ can be expressed as follows:

$$\mathbf{y}(m) = \sum_{i=0}^{m} \boldsymbol{\gamma}(i)\mathbf{u}(i) + \boldsymbol{\varepsilon} \tag{4}$$

where $\boldsymbol{\gamma}(i)=\mathbf{C}(m)\boldsymbol{\Phi}(m,i)\mathbf{B}(i)$, $\boldsymbol{\gamma}(0)=\mathbf{C}(m)\Phi(m,0)$, and $\boldsymbol{\Phi}(m,i)=\mathbf{A}(m-1)\mathbf{A}(m-2),\ldots,\mathbf{A}(i)$ for $m>i$, and $\boldsymbol{\Phi}(i,i)=\mathbf{I}$. In Eq. (4), it is special case scenario when index $i=0$ since station number is supposed to start from 1 instead of 0. In fact, $\mathbf{u}(0)$ here is incorporated with the same information as $\mathbf{X}(0)$, which represents initial condition of the state vector [7], namely, the fabrication imperfection of the parts before the assembly starts.

Equation (4) can also be written as follows (for simplicity, index "$m$" of $\mathbf{y}$ is dropped):

$$\mathbf{y} = \begin{vmatrix} \boldsymbol{\gamma}(0) & \boldsymbol{\gamma}(1) & \ldots & \boldsymbol{\gamma}(m) \end{vmatrix} \cdot \begin{vmatrix} \mathbf{u}(0) \\ \mathbf{u}(1) \\ \ldots \\ \mathbf{u}(m) \end{vmatrix} + \boldsymbol{\varepsilon} \tag{5}$$

Equation (5) actually has the same form as Eq. (1) listed here again for convenience and labeled as Eq. (6)

$$\mathbf{y} = \boldsymbol{\Gamma}\mathbf{u} + \varepsilon \tag{6}$$

where $\mathbf{y}$ represents the model output (end-of-line measurement data) and it is an $n\times 1$ random vector with zero mean

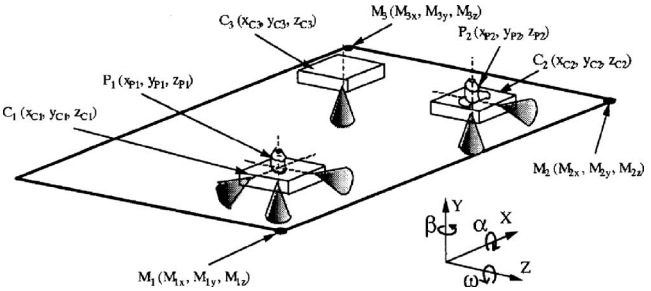


**Fig. 3 A schematic diagram of 3-2-1 fixture layout**

$$\boldsymbol{\Gamma} = \begin{vmatrix} \boldsymbol{\gamma}(0) & \boldsymbol{\gamma}(1) & \ldots & \boldsymbol{\gamma}(m) \end{vmatrix} \tag{7}$$

is an $n\times p$ matrix. It is the model parameter and represents a collection of fault patterns related to fixture and/or part mating errors. Matrix $\boldsymbol{\Gamma}$ is determined by the fixture layout and the distribution and number of measurement devices at all the stations, and it presents a total of $n$ measurements and $p$ error sources

$$\mathbf{u} = \begin{vmatrix} \mathbf{u}(0)' & \mathbf{u}(1)' & \ldots & \mathbf{u}(m)' \end{vmatrix}' \tag{8}$$

is a $p\times 1$ random vector and represents the model input of error sources from part fabrication, part mating features and fixture locators. These errors are assumed to be independent from each other

$$\boldsymbol{\varepsilon} = \sum_{i=1}^{m} \mathbf{C}\boldsymbol{\Phi}(m,i)\mathbf{w}(i) + \mathbf{v}(m) \tag{9}$$

is a $p\times 1$ random vector, which is the combination of process noise and measurement noise in the assembly process.

**2.2 Incorporation of Generic "3-2-1" Fixture Layout Into the State Space Model.** Ding et al. [22] applied the state space model to build a variation propagation model for multistation assembly processes. Their method simplifies the fixturing scheme as "0-2-1" (2D) instead of the generic "3-2-1" (3D). However, it does not consider part mating feature errors and includes only lap joints between assembled parts. Therefore, 3D variation propagation models are necessary for applications of actual assembly processes. Figure 3 shows a typical 3-2-1 fixture scheme for automotive sheet metal assembly. The model employed in this paper is based on the newly developed 3D variation propagation model for rigid parts, which takes into consideration both fixture locator errors and part mating feature errors [28,29].

In Eq. (2), matrix $\mathbf{A}(i-1)$ reflects the impact of locating scheme changes between stations on the variation of parts. The fundamental model, which provides the relationship between tolerance input and output variation at each station, is given by matrix $\mathbf{B}(i)$. In the following analysis, the process used to obtain matrix $\mathbf{B}(i)$ is explained briefly. For more details, please refer to Huang et al. [28,29].

The 3D variation propagation model considers a 3-2-1 fixture layout and various types of planar mating features, such as lap joint, butt joint, and T joint, among others. Figure 4 illustrates the generic 3-2-1 fixture setup. The locators $P_1$ to $P_6$ define three orthogonal planes: primary plane ($P_1$, $P_2$, and $P_3$), secondary plane ($P_4$ and $P_5$), and tertiary plane ($P_6$), respectively. Point $P_r$ is chosen as the reference point to describe the rigid-body variation of the entire part. The relationship between the errors of the six locators and point $P_r$ is derived using a kinematical model represented by matrix $\mathbf{F_s}$ in Eq. (10). $\mathbf{F_s}$ is solely determined based on the fixture locator layout information. Thus, given the fixture locator error $\Delta f$, the deviation of rigid part $\Delta P_r$ can be calculated using Eq. (10).

In some cases, the three locators, $P_1$, $P_2$, and $P_3$ in Fig. 4, which define the primary plane, are provided by part mating features,

instead of fixture locators. Equation (10) provides a generic unified model for both part mating errors and fixture locator errors. It shows that the part-to-part mating errors can also be represented in the same framework by considering them as virtual fixture locators. Therefore, this 3D variation propagation model includes both in-plane four-way/two-way induced deviation as well as out-of-plane deviation due to the three fixture locator errors or part mating feature errors

$$\mathbf{\Delta P_r} = \begin{bmatrix} \Delta x \\ \Delta y \\ \Delta z \\ \Delta \alpha \\ \Delta \beta \\ \Delta \gamma \end{bmatrix}_r = \mathbf{F_s \Delta f} = \begin{bmatrix} \frac{D_{y5r}}{D_{y54}} & \frac{D_{yr4}}{D_{y54}} & 0 & \frac{D_{zr4}D_{y32}}{R} & \frac{D_{zr4}D_{y13}}{R} & \frac{D_{zr4}D_{y21}}{R} \\ \frac{D_{xr6}}{D_{y54}} & \frac{D_{x6r}}{D_{y54}} & 1 & \frac{D_{z6r}D_{x32}}{R} & \frac{D_{z6r}D_{x13}}{R} & \frac{D_{z6r}D_{x21}}{R} \\ 0 & 0 & 0 & E & F & H \\ 0 & 0 & 0 & \frac{D_{x32}}{R} & \frac{D_{x13}}{R} & \frac{D_{x21}}{R} \\ 0 & 0 & 0 & \frac{D_{y32}}{R} & \frac{D_{y13}}{R} & \frac{D_{y21}}{R} \\ \frac{1}{D_{y54}} & \frac{-1}{D_{y54}} & 0 & 0 & 0 & 0 \end{bmatrix} \cdot \begin{bmatrix} \Delta x_4 \\ \Delta x_5 \\ \Delta y_6 \\ \Delta z_1 \\ \Delta z_2 \\ \Delta z_3 \end{bmatrix} \tag{10}$$

where $\mathbf{\Delta P_r}$ is the deviation of reference point $r$ chosen to represent the rigid-body part, and vector $[\Delta x_4, \Delta x_5, \Delta y_6, \Delta z_1, \Delta z_2, \Delta z_3]'$ represents the deviation of the six fixture locators (Fig. 4). $D_{xij}=(x_i-x_j)$, $D_{yij}=(y_i-y_j)$, $R=D_{x21}D_{y31}-D_{x31}D_{y21}$, $E=1+(D_{x1r}D_{y32}+D_{y1r}D_{x23})/R$, $F=(-D_{x1r}D_{y31}+D_{y1r}D_{x31})/R$, and $H=(D_{x1r}D_{y21}-D_{y1r}D_{x21})/R$. $x_i$ and $y_i$ represent $X$ and $Y$ coordinates of locating point $P_i$ in Fig. 4 ($1 \le i \le 6$).

Figure 5 depicts a typical assembly application that includes part to part mating error. For example, among the six locators of part 3, $P_{35}$ and $P_{34}$, which define the secondary plane, and $P_{36}$, which defines the tertiary plane, are provided by physical fixture locators. However, $P_{31}$, $P_{32}$, and $P_{33}$, which define the primary plane, are actually from the part to part mating feature between part 2 and part 3 (butt joint).

In this 3D variation propagation model, the generic 3-2-1 fixture modeling is encapsulated into the framework of the state space model, and input matrix **u** includes both fixture locator errors and part mating feature errors. Therefore, the variation propagation model applied in this paper is a significant enhancement of the model presented by Ding et al. [22].

The final output of the variation propagation model as represented in Eq. (6) depicts that even for a very complex multistation assembly process, the state space model is capable of capturing the linear relationship between the deviations of error sources and the measurements. This linear relationship plays a critical role in multiple fault diagnosis for a multistation assembly process.

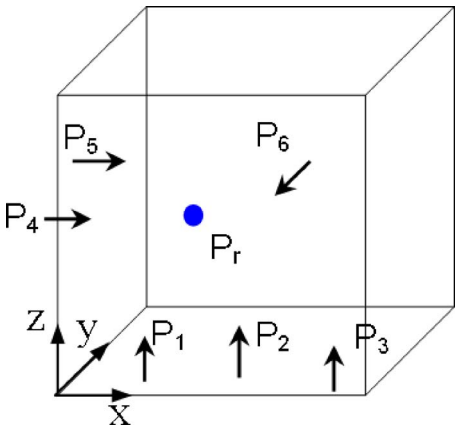


**Fig. 4 General 3-2-1 fixture layout**

## 3 Multiple Fault Diagnosis Using Orthogonal Diagonalization Analysis

The state space model reveals the linear relationship between error sources and measurements using matrix $\mathbf{\Gamma}$ (Eq. (6)), which contains all potential fault patterns. Each fault pattern is, in fact, a column of the matrix, namely, a vector. All these vectors form an affine space. By projecting the measurement data into the affine space, the corresponding variations of the error sources can be identified.

**3.1 Orthogonal Diagonalization Based on Principle Component Analysis.** The output of the state space model, namely, Eq. (6) can be rewritten as

$$\mathbf{y} = \mathbf{Me} + \boldsymbol{\varepsilon} \tag{11}$$

where vector $\mathbf{e}=[e_1, e_2, \ldots, e_p]'$ is a $p \times 1$ random vector with zero mean and unit variance, converted from vector **u** in Eq. (6). $\boldsymbol{\varepsilon}=[\varepsilon_1, \varepsilon_2, \ldots, \varepsilon_p]'$ is an $n \times 1$ random vector with zero mean and variance $\sigma^2$, and independent of **e**.

Assume that in Eq. (11), **M** is an $n \times p$ ($n > p$) matrix with linearly independent columns. Therefore, matrix **M** has full column rank. Each column of **M** (Eq. (12)) represents a fault pattern associated with one error source. Similar to matrix $\mathbf{\Gamma}$, matrix **M** also represents $n$ measurements and $p$ error sources in the assembly process

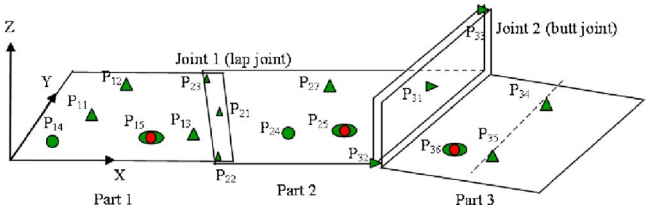


**Fig. 5 3D assembly with part-to-part mating error**

$$\mathbf{M} = \begin{bmatrix} m_{11} & m_{12} & \cdots & m_{1p} \\ m_{21} & \cdots & \cdots & \cdots \\ \cdots & \cdots & \cdots & \cdots \\ m_{n1} & \cdots & \cdots & m_{np} \end{bmatrix} \tag{12}$$

Next, rearrange Eq. (11), normalize each column of matrix **M**, and convert it to matrix **J**. Then, multiply the complementary ratio to vector **e**, and convert it to vector **b**. Consequently, Eq. (11) becomes Eq. (13). Each column of **J** is a unit vector. The deviation of each fault is completely contained in each component of vector **b**

$$\mathbf{y} = \mathbf{Jb} + \boldsymbol{\varepsilon} \tag{13}$$

From Eq. (11), covariance matrix of **y** can be represented as

$$\boldsymbol{\Sigma}_{\mathbf{y}} = \mathbf{E}[(\mathbf{Me} + \boldsymbol{\varepsilon})(\mathbf{Me} + \boldsymbol{\varepsilon})'] = \mathbf{MM}' + \sigma^2\mathbf{I} \tag{14}$$

By using PCA method, the following relationship holds:

$$\boldsymbol{\Sigma}_{\mathbf{y}} = \mathbf{Z}_k[\boldsymbol{\Lambda}_k - \sigma^2\mathbf{I}]\mathbf{Z}_k' + \sigma^2\mathbf{I} \tag{15}$$

where $\mathbf{Z}_k = [\mathbf{z_1}, \mathbf{z_2}, \ldots, \mathbf{z}_k]$ includes the eigenvectors, and $\boldsymbol{\Lambda}_k = \mathbf{diag}[\lambda_1, \lambda_2, \ldots, \lambda_k]$ includes the corresponding eigenvalues. $k$ is the number of dominant eigenvalues and can be determined using the method presented by Apley and Shi [19]. $\sigma^2$ can be estimated from the smallest $n-k$ eigenvalues.

Assume that after PCA analysis, the number of measurements is still greater than the number of error sources, namely, $k > p$. Based on Eqs. (14) and (15), we have

$$\mathbf{MM}' = \mathbf{Z}_k[\boldsymbol{\Lambda}_k - \sigma^2\mathbf{I}]\mathbf{Z}_k'$$

Thus, the following relationship can be derived:

$$\mathbf{M} = \mathbf{Z}_k[\boldsymbol{\Lambda}_k - \sigma^2\mathbf{I}]^{1/2}\mathbf{Q} \tag{16}$$

where **Q** is an arbitrary orthonormal matrix.

From Eqs. (11) and (13), we have

$$\mathbf{Jb} = \mathbf{Me} \tag{17}$$

Replace matrix **M** in Eq. (17) with Eq. (16), the following equation can be obtained:

$$[\boldsymbol{\Lambda}_k - \sigma^2\mathbf{I}]^{1/2}\mathbf{Qe} = \mathbf{Z}_k^{-1}\mathbf{Jb} = \mathbf{Nb} \tag{18}$$

where

$$\mathbf{N} = \mathbf{Z}_k^{-1}\mathbf{J} \tag{19}$$

Since $\mathbf{Z}_k$ is orthonormal and **J** is normalized with full column rank, **N** is still normalized with full column rank. **e** is a unit variance vector. Thus, we can obtain the following relationship:

$$\mathbf{N}\,\mathbf{Cov}(\mathbf{b})\mathbf{N}' = [\boldsymbol{\Lambda}_k - \sigma^2\mathbf{I}] \tag{20}$$

where **Cov** represents covariance of a matrix. Matrix **N** is applied to perform orthogonal diagonalization to both sides of Eq. (20), and the orthogonally diagonal form is obtained as follows:

$$\mathbf{Cov}(\mathbf{b}) = \mathbf{N}^{-1}[\boldsymbol{\Lambda}_k - \sigma^2\mathbf{I}](\mathbf{N}^{-1})' \tag{21}$$

The inverse function in Eqs. (18), (19), and (21) is the Moore–Penrose inverse. After a simple conversion, Eq (21) becomes

$$\mathbf{Cov}(\mathbf{b}) = \{[\mathbf{N}^{-1}[\boldsymbol{\Lambda}_k - \sigma^2\mathbf{I}](\mathbf{N}^{-1})']^{-1}\}^{-1} = (\mathbf{N}'[\boldsymbol{\Lambda}_k - \sigma^2\mathbf{I}]^{-1}\mathbf{N})^{-1} \tag{22}$$

Let $\sigma_{b_i}$ $(1 \le i \le p)$ represent the standard deviation of each of the error sources (i.e., each component of vector **b**) and expand Eq. (22), to derive the following expression:

$$\begin{bmatrix} \sigma_{b_1}^2 & 0 & \cdots & 0 \\ 0 & \sigma_{b_2}^2 & \cdots & \cdots \\ \cdots & \cdots & \cdots & \cdots \\ 0 & \cdots & \cdots & \sigma_{b_p}^2 \end{bmatrix} = \begin{bmatrix} \dfrac{n_{11}^2}{\lambda_1 - \sigma^2} + \dfrac{n_{21}^2}{\lambda_2 - \sigma^2} + \cdots + \dfrac{n_{k1}^2}{\lambda_k - \sigma^2} & 0 & \cdots & 0 \\ \cdots & \cdots & \cdots & \cdots \\ \cdots & \cdots & \cdots & \cdots \\ 0 & \cdots & \cdots & \dfrac{n_{1p}^2}{\lambda_1 - \sigma^2} + \dfrac{n_{2p}^2}{\lambda_2 - \sigma^2} + \cdots + \dfrac{n_{kp}^2}{\lambda_k - \sigma^2} \end{bmatrix}^{-1} \tag{23}$$

Finally, the variances of all error sources can be obtained, namely,

$$\begin{cases} \sigma_{b_1}^2 = \dfrac{1}{\dfrac{n_{11}^2}{\lambda_1 - \sigma^2} + \dfrac{n_{21}^2}{\lambda_2 - \sigma^2} + \cdots + \dfrac{n_{k1}^2}{\lambda_k - \sigma^2}} \\ \sigma_{b_2}^2 = \dfrac{1}{\dfrac{n_{12}^2}{\lambda_1 - \sigma^2} + \dfrac{n_{22}^2}{\lambda_2 - \sigma^2} + \cdots + \dfrac{n_{k2}^2}{\lambda_k - \sigma^2}} \\ \cdots \\ \sigma_{b_p}^2 = \dfrac{1}{\dfrac{n_{1p}^2}{\lambda_1 - \sigma^2} + \dfrac{n_{2p}^2}{\lambda_2 - \sigma^2} + \cdots + \dfrac{n_{kp}^2}{\lambda_k - \sigma^2}} \end{cases} \tag{24}$$

where $n_{ij}$ is a component of fault pattern matrix **N**. Assume $\boldsymbol{n}_i = [n_{1i}, n_{2i}, \ldots, n_{ki}]'$ is the $i$th fault pattern ($i$th column of matrix **N**), and the corresponding variance is $\sigma_{b_i}^2$, where $1 < i < p$. From Eq. (24), we can have

$$\frac{(\sigma_{b_i} n_{1i})^2}{\lambda_1 - \sigma^2} + \frac{(\sigma_{b_i} n_{2i})^2}{\lambda_2 - \sigma^2} + \cdots + \frac{(\sigma_{b_i} n_{ki})^2}{\lambda_k - \sigma^2} = 1 \tag{25}$$

This is a standard hyper ellipse representation. In fact, the vector of $[\sigma_{b_i} n_{1i}, \sigma_{b_i} n_{2i}, \ldots, \sigma_{b_i} n_{ki}]'$ represents a point on the boundary of the hyper ellipse. Since $\mathbf{d_i}$ is a unit vector, the length of the vector can calculated as

$$\|(\sigma_{b_i}\mathbf{n}_i)\| = \sqrt{(\sigma_{b_i} n_{1i})^2 + (\sigma_{b_i} n_{2i})^2 + \cdots + (\sigma_{b_i} n_{ki})^2} = \sigma_{b_i} \tag{26}$$

Thus, Eq. (26) is the standard deviation of the corresponding error source. Consequently, the deviation of vector **b** (Eq. (13)) can be obtained.

**3.2 Analysis of Geometric Factor Effect.** By applying the PCA-based orthogonal diagonalization, the deviation of vector **b** can be identified using measurement data **y** (Eq. (13)). However, the final goal of fault diagnosis is to identify the variation of **u** in Eq. (6). By comparing Eqs. (6) and (13), we can have the following expression:

$$\mathbf{y} = \boldsymbol{\Gamma}\mathbf{u} + \boldsymbol{\varepsilon} = \boldsymbol{\Gamma}\mathbf{G}\mathbf{G}^{-1}\mathbf{u} = \mathbf{Jb} + \boldsymbol{\varepsilon} \tag{27}$$

where **J** is a normalized matrix and

$$\mathbf{J} = \mathbf{\Gamma G} \tag{28}$$

$$\mathbf{b} = \mathbf{G}^{-1}\mathbf{u} \tag{29}$$

$$\mathbf{G} = \begin{bmatrix} \frac{1}{g_1} & \mathbf{0} & \cdots & \mathbf{0} \\ \mathbf{0} & \frac{1}{g_2} & \cdots & \mathbf{0} \\ \cdots & \cdots & \cdots & \cdots \\ \mathbf{0} & \mathbf{0} & \cdots & \frac{1}{g_p} \end{bmatrix} \tag{30}$$

$$g_i = \|\mathbf{\Gamma}(i)\| \quad 1 < i < p \tag{31}$$

where $\mathbf{\Gamma}(i)$ is the $i$th column of fault pattern matrix $\mathbf{\Gamma}$. From the state space modeling process, it can be seen that $g_i$ in Eq. (30) is determined by the geometric structure of the fixture and is thereby, termed as "geometric factor."

After further investigation of Eq. (29), it is clear that the vector $\mathbf{b}$ consists of both the original deviation of each error sources expressed by vector $\mathbf{u}$ as well as the effect of geometric factor $\mathbf{G}$. Therefore, Eq. (29) can be rewritten as follows:

$$\mathbf{u} = \mathbf{Gb} \tag{32}$$

Consequently, we have,

$$\mathbf{Cov}(\mathbf{u}) = \mathbf{G} \bullet \mathbf{Cov}(\mathbf{b}) \bullet \mathbf{G}' \tag{33}$$

where $\mathbf{Cov}(\mathbf{b})$ can be obtained using Eq. (23). The final result $\mathbf{Cov}(\mathbf{u})$ contains the original variations of all the error sources ($\mathbf{u}$ in Eq. (6)) since the effect of geometrical factor $\mathbf{G}$ has been filtered out.

**3.3 Statistical Analysis of Root Cause Estimation.** Using Eq. (32), the variations of all the error sources can be estimated. However, still to be identified are the root causes, i.e., large variations of fixture locators and/or part mating features, which result in unacceptable high variation of KPCs.

The root causes can be determined by using a hypothesis test on actual variation and tolerance specification of each error source. The interpretation of the test is that for each root cause, its actual variance shall be statistically greater than the variance of tolerance specification. The hypothesis can be formulated as follows:

$$\begin{aligned} &\mathbf{H_0}: \sigma^2_{u(i)} = \sigma^2_{u(i)\_\text{spec}} \\ &\mathbf{H_1}: \sigma^2_{u(i)} > \sigma^2_{u(i)\_\text{spec}} \end{aligned} \quad i = 1, \ldots, p \tag{34}$$

where $\sigma^2_{u(i)}$ represents the actual variance of error source $u_i$. $\sigma^2_{u(i)\_\text{spec}}$ is the tolerance specification variance of error source $u_i$. Assume that $S_{u(i)}$ is the estimated variance of error source $u_i$ based on $L$ samples of measurements, and then we can have

$$\frac{(L-1)S_{u(i)}}{\chi^2_{\alpha,L-1}} < \sigma^2_{U(i)} < \frac{(L-1)S_{u(i)}}{\chi^2_{1-\alpha,L-1}} \tag{35}$$

Select a statistic $\boldsymbol{\chi}^2_{\mathbf{0}}$ as

$$\chi^2_0 = \frac{(L-1)S_{u(i)}}{\sigma^2_{u(i)\_\text{spec}}} \tag{36}$$

Thus, the null hypothesis $\mathbf{H_0}$ will be rejected if

$$\chi^2_0 > \chi^2_{\alpha,L-1} \tag{37}$$

Error source $u_i$ is a root cause and a significant contributor of the KPCs' variation if the null hypothesis is rejected. By conducting the hypothesis test for every error source, all the root causes can be determined.

**3.4 Geometrical Illustration.** In this section, an illustration using geometrical figures is provided to explain the procedures conducted in Sec. 3.2. Figure 6(*a*) describes the measurement data with a certain number of samples. Each dot represents a measurement, namely, the $\mathbf{y}$ in Eq. (11). If the distributions of all the error sources are normal, then the measurements, which are linear combinations of the error sources, shall also be normally distributed. Graphically, measurements disperse in a high dimensional space can be shown as a hyper ellipse as depicted by Fig. 6(*a*). Figure 6(*b*) shows the hyper ellipse whose projections on its major axes are the variations of the measurement data in the directions of the major axes. Therefore, the hyper ellipse also graphically represents the covariance matrix structure of the measurement data.

Each fault pattern is represented using a vector, which is one of the columns of matrix $\mathbf{J}$ in Eq. (13). Figure 6(*b*) shows two fault pattern vectors marked as $FP_1$ and $FP_2$, respectively. These two vectors form an affine space. The resulting eigenvectors of PCA analysis from the measurement data provides the directions of the major axes of the hyper ellipse, which are expressed by matrix $\mathbf{Z}_k$ in Eq. (15). By applying the rotational transformation (determined by $\mathbf{Z}_k^{-1}$, the inverse function here is the Moore–Penrose inverse) to

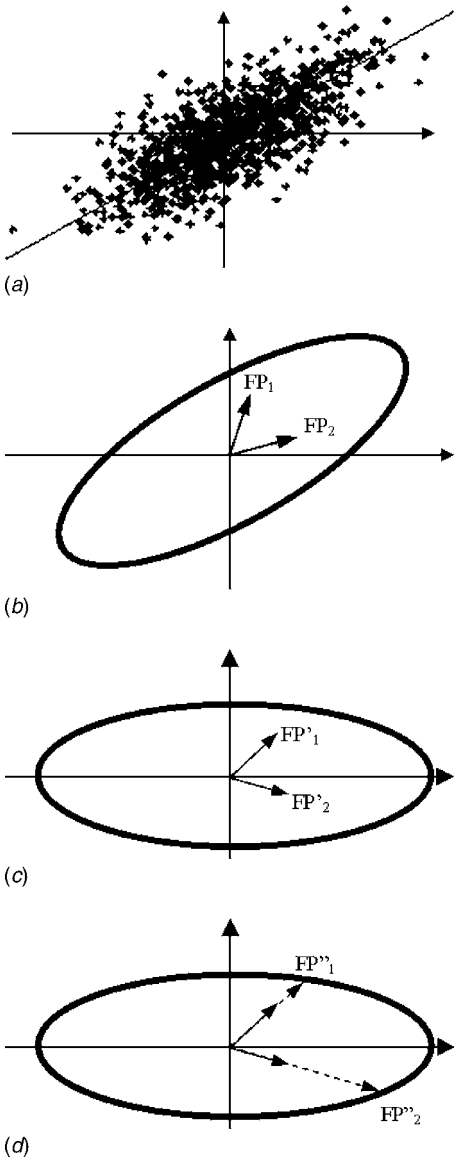


**Fig. 6 Procedure of the proposed fault diagnosis method: (*a*) Original measurement data, (*b*) hyper ellipse structure of the covariance matrix, (*c*) orthogonal diagonalization for the hyper ellipse, and (*d*) identification of the variations of the faults**

both the hyper ellipse and the affine space spanned by $FP_1$ and $FP_2$, the hyper ellipse will have a standard form displayed as shown in Fig. 6(*c*). Correspondingly, $FP_1$ and $FP_2$, become $FP_1'$ and $FP_2'$, respectively. This process is termed as orthogonal diagonalization. After this process, the diagonal covariance matrix of vector **b** is obtained and is expressed as Eq. (22).

Since the transformed hyper ellipse has a standard form, it is easy to calculate the projection of the hyper ellipse to axes of the affine space. As shown in Fig. 6(*d*), the unit vector $FP_1'$ and $FP_2'$ are extended and intersected with the hyper ellipse. The resulting vectors obtained from the intersected points are represented as $FP_1''$ and $FP_2''$, respectively, which are accurate projections of the hyper ellipse to the two axes of the affine space. The lengths of the vectors $FP_1''$ and $FP_2''$ represent the variations of the corresponding error sources, which are represented by vector **b** in Eq. (13). This can be explained using Eqs. (25) and (26).

## 4 Comparison to Existing Methods

In this section, a comparison analysis is conducted between the proposed method in this paper with existing methods to highlight the uniqueness of the new method.

**4.1 Comparison to the Least-Squares Estimation and the Maximum Likelihood Estimation.** By plugging Eq. (19) into Eq. (21), we have

$$\mathbf{Cov}(\mathbf{b}) = \mathbf{J}^{-1}\mathbf{Z}_k[\Lambda_k - \sigma^2\mathbf{I}]\mathbf{Z}_k^{-1}(\mathbf{J}^{-1})' \tag{38}$$

By utilizing the PCA results in Eq. (15), Eq. (38) becomes

$$\mathbf{Cov}(\mathbf{b}) = \mathbf{J}^{-1}\,\mathbf{Cov}(\mathbf{y}_1)(\mathbf{J}^{-1})' \tag{39}$$

where $\mathbf{Cov}(\mathbf{y}_1) = \boldsymbol{\Sigma}_\mathbf{y} - \sigma^2\mathbf{I}$, which is the covariance matrix of the measurement **y** after PCA processing. Furthermore, we have

$$\mathbf{b} = \mathbf{J}^{-1}\mathbf{y}_1 \tag{40}$$

Since the inverse function in Eq. (40) is the Moore–Penrose inverse, Eq. (40) takes the following form:

$$\mathbf{b} = (\mathbf{J}'\mathbf{J})^{-1}\mathbf{J}'\mathbf{y}_1 \tag{41}$$

in which the inverse function is a standard one. Equation (41) illustrates that the proposed method is essentially a least-squares method.

The uniqueness of the proposed method is that prior to conducting the least-squares estimation, a coordinate transformation is performed. The transformation expressed as $\mathbf{Z}_k^{-1}$ (Eq. (38)) is a rotation operation determined by eigenvectors of the measurement data. After this transformation, the covariance matrix of measurement data **y** becomes diagonal. In other words, the individual measurements are uncorrelated with each other. This is graphically illustrated in Figs. 6(*b*) and 6(*c*). The advantage of this method is that the variation estimation for each fault is solely determined by the fault pattern (one column of matrix **J** in Eq. (13) or matrix **N** in Eq. (19)) of the corresponding fault itself. This can be seen from Eq. (26). This makes the variation estimation for individual error source independent.

For the ordinary least-squares method, because the measurement data are correlated, the estimation of each fault depends on the whole structure of all the fault patterns (all columns of matrix **J** Eq. (13) or matrix **N** in Eq. (19)).

In a complex manufacturing process, it is not unusual that the complete design and process information is not available to quality engineers. Therefore, it is often the case that a completed fault pattern library (matrix **J** in Eq. (13) or matrix **N** in Eq. (19)) cannot be obtained. Under this circumstance, our proposed method can still accurately estimate the variance of the faults whose patterns are already identified regardless of other unidentified faults. However, for the ordinary least-squares method, the estimation will involve high errors since each fault is dependent on all fault patterns. Furthermore, even if a complete set of fault patterns is available, the inaccuracy of a single fault pattern may cause the estimation errors of other faults using the ordinary least-squares estimation. Nevertheless, in the proposed method, due to the property of variation estimation independence, the inaccuracy of a single fault pattern will not cause errors to the estimation of other faults.

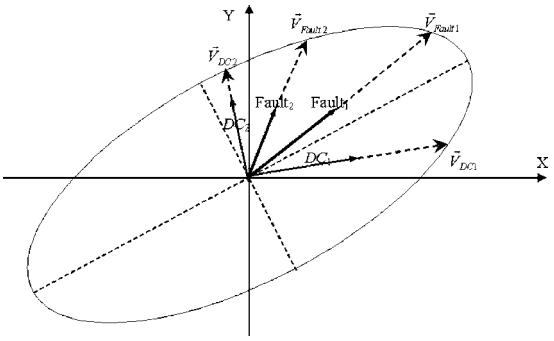


**Fig. 7 Illustration of the difference between the proposed method and DCA method**

The proposed method also presents the same advantage as mentioned above when using maximum likelihood estimation since the latter also requires complete fault patterns information.

**4.2 Comparison to DCA Method.** The DCA method developed by Camelio and Hu [8] has similar strategies for multiple fault diagnosis, namely, applying projection of the measurement data onto fault patterns so as to estimate the variation of error sources. Because fault patterns are not necessarily orthogonal to each other, the Pythagorean theorem cannot be directly applied to decompose the variations of error sources. In order to solve this issue, DCA uses Schmidt transformation to generate a set of orthogonal vectors from the original fault patterns. Therefore, the covariance matrix of measurement data can be projected to the generated orthogonal vectors based on the Pythagorean theorem.

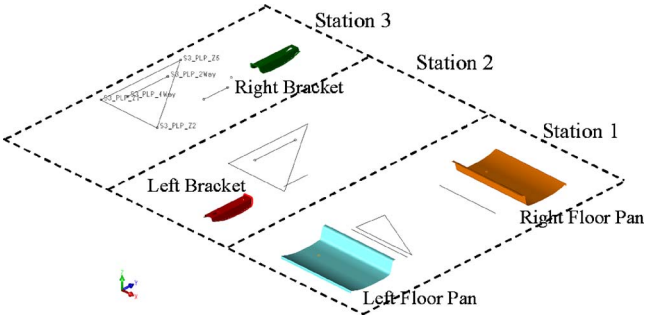


**Fig. 8 An example of multistation assembly process**

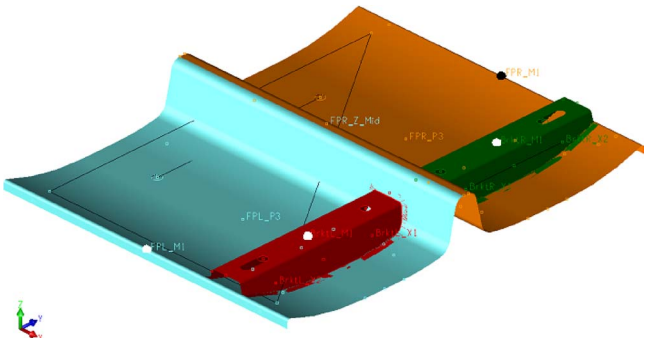

**Fig. 9 Final assembled product through multistation assembly process**

**Table 2 Generated fault patterns in station 3 using state space model**

| Faults / Measurements | $FP_1$ | $FP_2$ | $FP_3$ | $FP_4$ | $FP_5$ | $FP_6$ | $FP_7$ | $FP_8$ | $FP_9$ |
|---|---|---|---|---|---|---|---|---|---|
| FPL_M1_X | −0.060 | 0.060 | 0.000 | −1.588 | 0.588 | 0.000 | 0.000 | 0.000 | 0.000 |
| FPL_M1_Y | −0.043 | 0.000 | 0.043 | −0.523 | 0.523 | −1.000 | 0.000 | 0.000 | 0.000 |
| FPL_M1_Z | −0.551 | −0.500 | 0.051 | 0.000 | 0.000 | 0.000 | 0.000 | 0.000 | 0.000 |
| FPL_P1_X | 0.000 | 0.000 | 0.000 | −1.119 | 0.119 | 0.000 | 0.000 | 0.000 | 0.000 |
| FPL_P1_Y | 0.000 | 0.000 | 0.000 | −1.394 | 1.394 | −1.000 | 0.000 | 0.000 | 0.000 |
| FPL_P1_Z | 0.312 | −1.125 | −0.187 | 0.000 | 0.000 | 0.000 | 0.000 | 0.000 | 0.000 |
| FPL_P2_X | 0.000 | 0.000 | 0.000 | −0.881 | −0.119 | 0.000 | 0.000 | 0.000 | 0.000 |
| FPL_P2_Y | 0.000 | 0.000 | 0.000 | −1.394 | 1.394 | −1.000 | 0.000 | 0.000 | 0.000 |
| FPL_P2_Z | 0.432 | −1.125 | −0.307 | 0.000 | 0.000 | 0.000 | 0.000 | 0.000 | 0.000 |
| FPL_P3_X | 0.000 | 0.000 | 0.000 | −1.000 | 0.000 | 0.000 | 0.000 | 0.000 | 0.000 |
| FPL_P3_Y | 0.000 | 0.000 | 0.000 | −0.523 | 0.523 | −1.000 | 0.000 | 0.000 | 0.000 |
| FPL_P3_Z | −0.253 | −0.500 | −0.247 | 0.000 | 0.000 | 0.000 | 0.000 | 0.000 | 0.000 |
| FPR_M1_X | −0.060 | 0.060 | 0.000 | 0.588 | −1.588 | 0.000 | 0.000 | 0.000 | 0.000 |
| FPR_M1_Y | −0.043 | 0.000 | 0.043 | −0.523 | 0.523 | −1.000 | 0.000 | 0.000 | 0.000 |
| FPR_M1_Z | 0.551 | −0.500 | −1.051 | 0.000 | 0.000 | 0.000 | 0.000 | 0.000 | 0.000 |
| FPR_Z7_X | 0.000 | 0.000 | 0.000 | −0.119 | −0.881 | 0.000 | 0.000 | 0.000 | 0.000 |
| FPR_Z7_Y | 0.000 | 0.000 | 0.000 | −1.394 | 1.394 | −1.000 | 0.000 | 0.000 | 0.000 |
| FPR_Z7_Z | 0.818 | −1.125 | −0.693 | 0.000 | 0.000 | 0.000 | 0.000 | 0.000 | 0.000 |
| FPR_P2_X | 0.000 | 0.000 | 0.000 | 0.119 | −1.119 | 0.000 | 0.000 | 0.000 | 0.000 |
| FPR_P2_Y | 0.000 | 0.000 | 0.000 | −1.394 | 1.394 | −1.000 | 0.000 | 0.000 | 0.000 |
| FPR_P2_Z | 0.938 | −1.125 | −0.813 | 0.000 | 0.000 | 0.000 | 0.000 | 0.000 | 0.000 |
| FPR_P3_X | 0.000 | 0.000 | 0.000 | 0.000 | −1.000 | 0.000 | 0.000 | 0.000 | 0.000 |
| FPR_P3_Y | 0.000 | 0.000 | 0.000 | −0.523 | 0.523 | −1.000 | 0.000 | 0.000 | 0.000 |
| FPR_P3_Z | 0.253 | −0.500 | −0.753 | 0.000 | 0.000 | 0.000 | 0.000 | 0.000 | 0.000 |
| BrktL_M1_X | −0.102 | 0.102 | 0.000 | −1.083 | 0.083 | 0.000 | 0.000 | 0.000 | 0.000 |
| BrktL_M1_Y | −0.072 | 0.000 | 0.072 | −0.999 | 0.999 | −1.000 | 0.000 | 0.000 | 0.000 |
| BrktL_M1_Z | 0.046 | −0.841 | −0.205 | 0.000 | 0.000 | 0.000 | 0.000 | 0.000 | 0.000 |
| BrktL_M2_X | −0.048 | 0.048 | 0.000 | −1.085 | 0.085 | 0.000 | 0.000 | 0.000 | 0.000 |
| BrktL_M2_Y | −0.034 | 0.000 | 0.034 | −1.104 | 1.104 | −1.000 | 0.000 | 0.000 | 0.000 |
| BrktL_M2_Z | 0.121 | −0.917 | −0.204 | 0.000 | 0.000 | 0.000 | 0.000 | 0.000 | 0.000 |
| BrktL_X2_X | −0.048 | 0.048 | 0.000 | −1.381 | 0.381 | 0.000 | 0.000 | 0.000 | 0.000 |
| BrktL_X2_Y | −0.034 | 0.000 | 0.034 | −1.104 | 1.104 | −1.000 | 0.000 | 0.000 | 0.000 |
| BrktL_X2_Z | −0.029 | −0.917 | −0.054 | 0.000 | 0.000 | 0.000 | 0.000 | 0.000 | 0.000 |
| BrktL_X1_X | −0.048 | 0.048 | 0.000 | −0.789 | −0.211 | 0.000 | 0.000 | 0.000 | 0.000 |
| BrktL_X1_Y | −0.034 | 0.000 | 0.034 | −1.104 | 1.104 | −1.000 | 0.000 | 0.000 | 0.000 |
| BrktL_X1_Z | 0.271 | −0.917 | −0.354 | 0.000 | 0.000 | 0.000 | 0.000 | 0.000 | 0.000 |
| BrktR_M1_X | −0.101 | 0.114 | 0.052 | −0.003 | −0.001 | −0.002 | −0.498 | −0.498 | 0.002 |
| BrktR_M1_Y | −0.021 | 0.019 | 0.024 | 0.000 | −0.002 | −0.001 | 0.000 | 0.000 | −0.999 |
| BrktR_M1_Z | 0.638 | −0.840 | −0.793 | 0.017 | 0.048 | 0.023 | −0.033 | −0.033 | −0.023 |
| BrktR_M2_X | −0.047 | 0.060 | 0.052 | −0.001 | −0.003 | −0.002 | −0.498 | −0.498 | 0.002 |
| BrktR_M2_Y | 0.021 | 0.019 | −0.018 | −0.005 | 0.004 | −0.001 | −0.169 | 0.169 | −0.999 |
| BrktR_M2_Z | 0.715 | −0.916 | −0.794 | 0.020 | 0.046 | 0.023 | −0.037 | −0.029 | −0.023 |
| BrktR_X2_X | −0.057 | 0.060 | 0.062 | 0.000 | −0.004 | −0.002 | 0.000 | −0.996 | 0.002 |
| BrktR_X2_Y | 0.021 | 0.019 | −0.018 | −0.005 | 0.004 | −0.001 | −0.169 | 0.169 | −0.999 |
| BrktR_X2_Z | 0.864 | −0.916 | −0.943 | 0.000 | 0.065 | 0.023 | −0.004 | −0.061 | −0.023 |
| BrktR_X1_X | −0.037 | 0.060 | 0.042 | −0.003 | −0.002 | −0.002 | −0.995 | 0.000 | 0.002 |
| BrktR_X1_Y | 0.021 | 0.019 | −0.018 | −0.005 | 0.004 | −0.001 | −0.169 | 0.169 | −0.999 |
| BrktR_X1_Z | 0.565 | −0.916 | −0.645 | 0.039 | 0.026 | 0.023 | −0.069 | 0.004 | −0.023 |

However, the newly generated orthogonal fault patterns are just approximations of the original ones. The error is not trivial in the case of correlated original fault patterns.

The method proposed in this paper adopts affine projection, which directly reveals the contributions of the error sources represented by the axes of the affine coordinate. It fully utilizes the characteristics of multivariate normal distribution of the measurement data (hyper ellipse) and directly calculates the variations of original fault patterns.

The ellipse in Fig. 7 illustrates the covariance matrix structure of the measurement data. Assume that there are two faults $\mathbf{Fault_1}$ and $\mathbf{Fault_2}$, which are not orthogonal and are different from the major axes of the ellipse. The proposed method can directly calculate accurate variations of the two faults, $\|\vec{\mathbf{V}}_{\mathbf{Fault1}}\|$ and $\|\vec{\mathbf{V}}_{\mathbf{Fault2}}\|$. The DCA method uses Schmidt transformation to obtain two orthogonal directions $\mathbf{DC_1}$ and $\mathbf{DC_2}$ based on the original fault patterns $\mathbf{Fault_1}$ and $\mathbf{Fault_2}$, respectively. $\mathbf{DC_1}$ and $\mathbf{DC_2}$ are approximations of original faults $\mathbf{Fault_1}$ and $\mathbf{Fault_2}$. Therefore, the variation of the two faults calculated using their method are $\|\vec{\mathbf{V}}_{\mathbf{DC1}}\|$ and $\|\vec{\mathbf{V}}_{\mathbf{DC2}}\|$, instead of $\|\vec{\mathbf{V}}_{\mathbf{Fault1}}\|$ and $\|\vec{\mathbf{V}}_{\mathbf{Fault2}}\|$. Figure 7 illustrates that the DCA method just provides an approximation of the variations of the original faults. In contrast, the proposed method is able to give a more accurate estimation of variations of the faults.

## 5 Case Studies

In order to validate the proposed methodology, 3DCS ANALYST software package is used to simulate actual assembly process [30]. The output from the 3DCS ANALYST shows results that represent deviations from design nominal for the defined measurement points (KPCs). In the following case study, the simulation results

**Table 3 Identified variations of the error sources**

| | Actual range of the error sources (mm) | Estimated range of the error sources (mm) | Relative discrepancy (%) |
|---|---|---|---|
| Fix3_Z(FPL_Z1) | 0.50 | 0.5097 | 1.910 |
| Fix3_Z(FPL_Z2) | 0.50 | 0.4906 | 1.924 |
| Fix3_Z(FPL_Z3) | 0.50 | 0.4890 | 2.249 |
| Fix3_X1(FP_4Way) | 0.50 | 0.5149 | 2.885 |
| Fix3_X1(FP_2Way) | 0.50 | 0.4778 | 4.654 |
| Fix3_Y1(FP_4Way) | 0.50 | 0.4859 | 2.912 |
| Fix3_Y2(BrktR_X1) | 1.00 | 1.0153 | 1.511 |
| Fix3_Y2(BrktR_X2) | 1.00 | 1.0007 | 0.071 |
| Fix3_Y2(BrktR_Y1) | 1.00 | 1.0044 | 0.437 |

are taken as measurement data to identify the variation of error sources.

Figure 8 shows a multistation variation propagation model in 3DCS ANALYST, which includes three stations, through which a total of four parts, namely, left floor pan, right floor pan, left bracket, and right bracket, are assembled. Figure 9 displays the final assembled product. The measurements are taken at station 3. Four points on each individual part are measured. Each measurement point is measured in $X$, $Y$, and $Z$ directions, respectively. Therefore, there are a total of 48 measurements taken at station 3.

For the model shown in Fig. 8, the fixture locator positions and locations of measurement devices are given. Therefore, the state space modeling presented in Sec. 2 can be applied to generate the explicit variation propagation model represented by matrix $\mathbf{\Gamma}$, which represents the linear relationship between the error sources and the measurements. The $\mathbf{\Gamma}$ dimension is $n \times p$, where $n=48$ (the number of measurements) and $p=45$ (the number of error sources, namely) in all 3 stations. Partial of matrix $\mathbf{\Gamma}$ is listed in Table 2, which corresponds to the fixture locator error sources in station 3. Associated with the nine fixture locators in station 3, the nine fault patterns are marked as $FP_1$–$FP_9$ in Table 2.

The 3DCS ANALYST model depicted in Fig. 8 simulates the actual assembly process with tolerance input shown in the second column of Table 3 (actual range of the tolerance contributors). By using the fault diagnosis method presented in Sec. 3, the variation of all the error sources can be identified. The identified variations of fixture locators at station 3 are listed in the third column (estimated range of the tolerance contributors) of Table 3. The largest relative error between estimated tolerance ranges and actual input ranges to the simulation is only 4.65%.

## 6 Discussion and Summary

An important assumption introduced in the proposed method is the number of measurements $n$ being greater than the number of error sources $p$ in Eq. (11) and matrix $\mathbf{M}$ having linearly independent columns. Additionally, after PCA analysis, the number of dominant eigenvalues $k$ is greater than the number of error sources $p$. These two assumptions play the same role that ensures the unique solution of error sources variations. Matrix $\mathbf{M}$ is converted from matrix $\mathbf{\Gamma}$ in Eq. (6), which is the output from the variation propagation model. Before the diagnostic method is applied, matrix $\mathbf{\Gamma}$ shall be analyzed first to eliminate the trivial columns (norm of the vectors are very small) and to identify the linear dependence among the columns. This type of analysis is termed diagnosability study. References [26,27] have developed corresponding approaches to handle diagnosability issues, which shall be combined together with the diagnostic method proposed in this paper.

An effective fault diagnosis methodology needs to simultaneously focus on modeling of variation propagation in complex manufacturing processes and root cause identification. Overemphasizing or ignoring either one will cause inaccuracy of estimation. This paper utilizes the state space model for variation propagation based on engineering principles in multistation assembly processes. The generic 3-2-1 fixturing scheme is taken into consideration. Therefore, both part mating errors and fixture locator errors are included into the model. With respect to measurement data analysis, by utilizing the multivariate normal distribution property, a PCA-based orthogonal diagonalization method is developed to transform the measurement data. In doing so, the variations of error sources can be identified accurately. The proposed method can still give an accurate estimation even if only partial fault pattern matrix $\mathbf{\Gamma}$ is known. This is because the variations of different error sources are uncorrelated and then they can be identified individually. Thus, it has a more flexible requirement than the widely used ordinary least-squares estimation and maximum likelihood estimation both of which require that fault patterns be included completely in matrix $\mathbf{\Gamma}$. The case study indicates that accurate estimation results can be obtained when the proposed method is applied to solve multiple fault diagnosis problems in a multistation assembly process.

## Acknowledgment

The authors gratefully acknowledge the financial support of the NIST Advanced Technology Program (ATP Cooperative Agreement No. 70NANB3H3054), U.S. National Science Foundation CAREER Award Grant No. NSF-DMII-0239244 and UK EPSRC Star Award.

## References

[1] Ceglarek, D., and Shi, J., 1995, "Dimensional Variation Reduction for Automotive Body Assembly," Manuf. Rev., **8**(2), pp. 139–154.
[2] Hu, S., and Wu, S. M., 1992, "Identifying Root Causes of Variation in Automobile Body Assembly Using Principal Component Analysis," Trans. North Am. Manuf. Res. Inst. SME, **20**, pp. 311–316.
[3] Ceglarek, D., Shi, J., and Wu, S., 1994, "A Knowledge-Based Diagnostic Approach for the Launch of the Autobody Assembly Process," ASME J. Eng. Ind., **116**(4), pp. 491–499.
[4] Ceglarek, D., and Shi, J., 1996, "Fixture Failure Diagnosis for the Autobody Assembly Using Pattern Recognition," ASME J. Eng. Ind., **118**(1), pp. 55–66.
[5] Apley, D. W., and Shi, J., 1998, "Diagnosis of Multiple Fixture Faults in Panel Assembly," ASME J. Manuf. Sci. Eng., **120**(4), pp. 793–801.
[6] Rong, Q., Ceglarek, D., and Shi, J., 2000, "Dimensional Fault Diagnosis for Compliant Beam Structure Assemblies," ASME J. Manuf. Sci. Eng., **122**(4), pp. 773–780.
[7] Ding, Y., Ceglarek, D., and Shi, J., 2002, "Fault Diagnosis of Multistage Manufacturing Processes by Using State Space Approach," ASME J. Manuf. Sci. Eng., **124**(2), pp. 313–322.
[8] Camelio, J. A., and Hu, S. J., 2004, "Multiple Fault Diagnosis for Sheet Metal Fixtures Using Designated Component Analysis," ASME J. Manuf. Sci. Eng., **126**(1), pp. 91–97.
[9] Koren, Y., Heisel, U., Jovane, F., Moriwaki, T., Pritschow, G., Ulsoy, G., and Brussel, H., 1999, "Reconfigurable Manufacturing Systems," CIRP Ann., **48**(2), pp. 527–540.
[10] Kong, Z., and Ceglarek, D., 2003, "Rapid Deployment of Reconfigurable Assembly Fixtures Using Workspace Synthesis and Visibility Analysis," CIRP Ann., **52**(1), pp. 13–16.
[11] Khan, A., Ceglarek, D., and Ni, J., 1998, "Sensor Location Optimization for Fault Diagnosis in Multi-Fixture Assembly Systems," ASME J. Manuf. Sci. Eng., **120**(4), pp. 781–792.

[12] Khan, A., Ceglarek, D., Shi, J., Ni, J., and Woo, T. C., 1999, "Sensor Optimization for Fault Diagnosis in Single Fixture System: A Methodology," ASME J. Manuf. Sci. Eng., **121**(1), pp. 109–117.
[13] Ding, Y., Kim, P., Ceglarek, D., and Jin, J., 2003, "Optimal Sensor Distribution for Variation Diagnosis in Multi-Station Assembly Processes," IEEE Trans. Rob. Autom., **19**(4), pp. 543–556.
[14] Djurdjanovic, D., and Ni, J., 2004, "Measurement Scheme Synthesis in Multi-Station Machining Systems," ASME J. Manuf. Sci. Eng., **126**(1), pp. 178–188.
[15] Ceglarek, D., and Shi, J., 1999, "Fixture Failure Diagnosis for Sheet Metal Assembly With Consideration of Measurement Noise," ASME J. Manuf. Sci. Eng., **121**(4), pp. 771–777.
[16] Rong, Q., Shi, J., and Ceglarek, D., 2001, "Adjusted Least Squares Approach for Diagnosis of Compliant Assemblies in the Presence of Ill-conditioned Problems," ASME J. Manuf. Sci. Eng., **123**(3), pp. 453–461.
[17] Barton, R. R., and Gonzalez-Barreto, D. R., 1996, "Process-Oriented Basis Representations for Multivariate Process Diagnosis," Qual. Eng., **9**, pp. 107–118.
[18] Chang, M., and Gossard, D. C., 1998, "Computational Method for Diagnosis of Variation-Related Assembly Problems," Int. J. Prod. Res., **36**, pp. 2985–2995.
[19] Apley, D. W., and Shi, J., 2001, "A Factor Analysis Method for Diagnosing Variability in Multivariate Manufacturing Processes," Technometrics, **43**(1), pp. 84–95.
[20] Apley, D. W., and Lee, H. Y., 2003, "Identifying Spatial Variation Patterns in Multivariate Manufacturing Processes: A Blind Separation Approach," Technometrics, **45**(3), pp. 220–234.
[21] Carlson, J. S., and Soderberg, R., 2003, "Assembly Root Cause Analysis: A Way to Reduce Dimensional Variation in Assembled Products," Int. J. Flex. Manuf. Sys., **15**(2), pp. 113–150.
[22] Ding, Y., Ceglarek, D., and Shi, J., 2000, "Modeling and Diagnosis of Multistage Manufacturing Processes: Part I: State Space Model," *Japan/USA Symposium on Flexible Automation*, July 23–26, Ann Arbor.
[23] Zhou, S., Chen, Y., and Shi, J., 2004, "Root Cause Estimation and Statistical Testing for Quality Improvement of Multistage Manufacturing Processes," IEEE. Trans. Autom. Sci. Eng., **1**(1), pp. 73–83.
[24] Djurdjanovic, D., and Ni, J., 2003, "Bayesian Approach to Measurement Scheme Analysis in Multi-Station Machining Systems," Proc. Inst. Mech. Eng., Part B, **217**, pp. 1117–1130.
[25] Ding, Y., Zhou, S., and Chen, Y., 2005, "A Comparison of Process Variance Estimation Methods for In-Process Dimensional Control," ASME J. Dyn. Syst., Meas., Control, **127**(1), pp. 69–79.
[26] Ding, Y., Shi, J., and Ceglarek, D., 2002, "Diagnosability Analysis of Multistage Manufacturing Processes," ASME J. Dyn. Syst., Meas., Control, **124**(1), pp. 1–13.
[27] Zhou, S., Ding, Y., Chen, Y., and Shi, J., 2003, "Diagnosability Study of Multistage Manufacturing Processes Based on Linear Mixed-Effects Models," Technometrics, **45**(4), pp. 312–325.
[28] Huang, W., Lin, J., Bezdecny, M., Kong, Z., and Ceglarek, D., 2006, "Stream-of-Variation Modeling I: A Generic 3D Variation Model for Rigid Body Assembly in Single Station Assembly Processes ASME Trans.," ASME J. Manuf. Sci. Eng., **130**(1), pp. 821–831.
[29] Huang, W., Lin, J., Kong, Z., and Ceglarek, D., 2006, "Stream-of-Variation Modeling II: A Generic 3D Variation Model for Rigid Body Assembly in Multi Station Assembly Processes," ASME J. Manuf. Sci. Eng., **130**(1), pp. 832–842.
[30] DCS, 2002, *3DCS-Analyst 6.2.2 User Manual*, Dimensional Control Systems, Inc., Troy, MI.